Journal of Constructional Steel Research 211 (2023) 108222

Contents lists available at ScienceDirect

Journal of Constructional Steel Research

journal homepage: www.elsevier.com/locate/jcsr

Vibration control of steel frames with setback irregularities equipped with semi-active tuned mass dampers

Seyed Amin Hosseini [a,1], Vahid Jahangiri [b,2], Ali Massumi [b,*,3]

[a] ISISE-Department of Civil Engineering, University of Coimbra, Portugal
[b] Kharazmi University, No.43, Dr. Mofatteh Ave., Tehran 15719-14911, Iran

ARTICLE INFO

Keywords:
Semi-active vibration control
Tuned mass damper
Setback buildings
Irregular steel frame
Vibration control

ABSTRACT

This paper presents a pioneering study on the seismic vibration control of steel moment-resisting frames (MRFs) with setback irregularities using semi-active tuned mass dampers (SATMDs). The research investigates the efficiency and the location of the SATMDs and compares their efficiency with traditional tuned mass dampers (TMDs) for the vibration control of setback structures with different vertical irregularities. To assess the nonlinear seismic performance of buildings with setbacks, various engineering demand parameters such as inter-story drift ratio, story displacement, story velocity, story acceleration, and base shear factor were analyzed under earthquake excitations. The results reveal that the use of SATMDs reduced the seismic response of irregular frames with setbacks. In addition, the efficiency of SATMDs in the control of setback frames was more than the regular frames. Also, the investigations showed that placement of the control systems at the roof level of the structure significantly reduced the structural vibration of irregular structures. It is noticeable that the use of these control devices requires more attention for structures with significant setbacks because, in some cases, the response of a structure with SATMDs can be greater than an uncontrolled structure.

1. Introduction

Semi-Active Tuned Mass Dampers (SATMDs) systems can be used to control the lateral response of a structure under seismic and wind loads [1–4]. In such approaches, the TMD is equipped with a semi-active (SA) system that provides time-varying damping. This type of vibration control device is known as a SATMD. While an active control system requires a significant source of external energy to efficiently decrease the structural response, a semi-active control system requires only a small amount of active energy to reduce the vibration of the structure. In addition, semi-active control systems can provide more reliable and cost-effective vibration control of civil structures than passive control systems [5–8].

Pinkaew and Fujino studied the effects of SATMDs under harmonic excitation and found that SATMDs were more cost-effective compared to active strategies and were more efficient than passive strategies [9]. Ground-hook tuned mass dampers (GHTMDs) are semi-active vibration control systems introduced by Setareh [10]. It has been observed that the efficiency of decreasing the seismic structural behavior using a GHTMD is greater than for conventional TMDs. Lin et al. investigated the seismic response control of structures using semi-active-friction TMDs (SAF-TMDs) and reported that the performance of SAF-TMDs was more efficient than passive-friction TMDs [11]. Lin et al. carried out an experimental study on structural control reduction and reported that the results of the theoretical and experimental studies were similar [12].

Chey et al. simulated a design concept for vibration control systems that are equipped with both passive TMDs (PTMDs) and SATMDs [2,13]. Chung et al. suggested a SATMD that includes a novel phase control algorithm and validated their suggestion with experimental studies [14]. Although PTMDs are sensitive to the device frequency ratio, sensitivity studies have shown that the performance of the SATMDs was more reliable than PTMDs. Furthermore, the efficiency of controlled structures with SATMDs was not limited to the controller frequency ratio.

Soto and Adeli found that the efficiency of decreasing the structural

* Corresponding author.
E-mail address: massumi@khu.ac.ir (A. Massumi).
[1] Ph.D. student in Steel and Composite Construction.
[2] Master graduate of Structural Engineering, Kharazmi University.
[3] Professor of Structural Engineering, Kharazmi University.

https://doi.org/10.1016/j.jcsr.2023.108222
Received 13 May 2023; Received in revised form 27 August 2023; Accepted 11 September 2023
Available online 16 September 2023

response depended on the frame rigidity and was greater for tall buildings [15]. The application of SATMDs by assessing parameters such as damping and stiffness to control the behavior of structures under the effects of an earthquake was studied by Sun and Nagarajaiah [1]. They found that SATMDs performed better than TMDs in controlling the seismic response of regular frames under the effects of near-fault earthquakes. Kim et al. studied the vibration control of buildings with SATMDs and reported that the SATMDs decreased the vibrations of structures, regardless of the earthquake parameters [16]. Bathaei et al. suggested innovative fuzzy algorithm control of structural responses using a SATMD+MR damper, which was applicable for both near-fault and far-field earthquakes [17].

Lu et al. investigated the effect of the mass ratio of TMDs on super high-rise structures to control structural vibration [18]. The vibration control of high-rise irregular reinforced concrete structures by TMDs was studied by Reddy et al. and the results showed that the performance of the TMDs did not change significantly with the addition of shear walls [19].

Elias et al. showed that TMDs efficiently reduce the acceleration response of structure more than the displacement of a tall building under the effect of wind and seismic loads [20,21]. Shih and Sung improved a special type of SATMD with an impulsive reaction [22]. Kim proposed an innovative method to simulate and evaluate the seismic response of structures with SATMDs using a recurrent neural network (RNN) [23]. The results showed that the RNN significantly increased the accuracy of the seismic response and decreased the cost of software analysis over conventional finite element methods. The performance of SATMDs to reduce the structural vibration of footbridges under synchronous lateral excitation was studied by Ferreira et al. [24]. Their results showed that SATMDs had a more efficient potential to reduce the vibrations of the structure compared to PTMDs.

The efficiency of SATMD to control the seismic response of eight-story structures with linear and nonlinear base isolation systems was studied by Wang et al. [25]. The results showed that the seismic response of the structures with SATMD devices has an effect on reducing both acceleration and displacements. In addition, Ghorbanzadeh et al. evaluated the seismic behavior of structures with SATMD by considering the Soil-Pile-Structure-Interaction (SPSI) [26]. The results showed that by considering SPSI, structures without SATMD experienced smaller responses compared to structures with SATMD.

In addition, previous studies reported that SATMD devices were efficient under both near-faults and far-field earthquakes [1]. Less acceleration and drift response under pulse-like seismic events was reported for the buildings equipped with SATMD devices [25]. Also, the efficiency of proposed SATMDs was better than active dampers [27].

The mass, stiffness, and strength distribution in the horizontal and vertical plans of a structure have significant effects on its seismic response under strong ground motions [28–30]. Irregularities such as structures with setbacks exhibit undesirable seismic behavior under strong earthquakes [31,32]. Several investigations on the inelastic seismic response of structures with setbacks indicate that, compared to regular frames, there was a noticeable change in the seismic response of frames with setbacks [31]. Shahrooz and Moehle carried out an analytical and experimental study on the response of steel structures with setbacks and proposed a lateral-load design procedure for such structures [28]. Karavasilis et al. studied the inelastic lateral response of plane steel moment resisting frames (MRFs) with setbacks under earthquake loads and presented a formula that considers the setback effects [33].

Furthermore, the seismic response of structures with setbacks that are located on the soft soil was more complex and should be considered when designing this type of structure [34]. Nievas and Sullivan proposed the use of a direct displacement-based design method for MRFs with setbacks [35]. A simple and economical procedure for evaluating the seismic performance of steel MRFs with setbacks that depend on reliability-performance-based methods was proposed by Pirizadeh and Shakib [36].

The seismic performance of structures with setbacks under pulse-like events was numerically studied by Mashhadi et al. [32,37]. The results show that the seismic behavior of structures with setbacks depends on the ratio of the pulse period to the structures' first mode period, (T_P/T_1). They suggested that in the situation in which $T_P/T_1 \leq 1$, the fragility curve of structures with setback irregularity should be evaluated by considering the original near-fault earthquakes. In addition, using the buckling-restrained braces to reduce the seismic behavior of irregular structures with setbacks was suggested by Tu et al. [38].

Buildings with setbacks could experience early yielding at some members due to their complex mode shapes and concentrated deformation. Reduction of the geometry along the height of the structure leads to a significant increase in the building's vulnerability under seismic loads [39]. The higher mode participation and seismic demand for buildings with a setback are more than regular buildings, however, in some standards, the seismic demand is underestimated [40]. In addition, compared to regular beguiling, the torsional response of a building with setback irregularity could increase up to two times [41]. Results of the seismic behavior of a 25-story building with setbacks show an increase in the IDR demand for irregular buildings [42]. Saadatkhah et al. proposed a formulation to calculate the fundamental period of structures by considering the different structural cicatrises along the story height [43]. One of the advantages of the suggested method is that the calculation process takes into account the height irregularities such as setbacks, and changes in the stiffness and strength of stories.

Recently, limited investigations studied the efficiency of vibration control systems to reduce the response of a structure with irregularity [44,45]. On one hand, previous studies reported that the setback has an efficient effect on the seismic behavior of structures. On the other hand, the efficiency of the SATMD dampers to control the vibration of regular structures was studied. For buildings with regularity in stories, the best location for the vibration control devices is at the roof levels, but, still, there is a gap for the location of dampers for buildings with setbacks which is required to be investigated. In addition, due to limitations in the space of the top story for the dampers with high levels of irregularities in height, the below stories can be selected for the absorber devices. To tackle these gaps, this research evaluated the efficiency of dampers by considering the level of irregularities in elevation and the location of dampers.

The current study investigated the vibration control of setback structures under the effect of seismic loads with the application of SATMDs. The vertical location of the SATMDs in high-rise steel frames having different setback configurations was examined. In addition, a comparison between the effects of TMD and SATMD devices will be presented to show the efficiency of SATMDs. To clarify the seismic behavior of controlled irregular structures with SATMDs, after introducing case study frames with different vertical irregularities (setbacks) and selected earthquake events, some key parameters including the inter-story drift ratio, story displacement, story velocity, story acceleration, and base shear factor under the effect of earthquake events will be presented.

2. Building frame models and ground motions

Ten ductile (special) steel MRFs, nine with different types of setbacks and one reference (regular) frame, were studied. They were located in Tehran in a highly active seismic zone site with a design acceleration coefficient of 0.35 g. They were designed following the Iranian Code of Practice for Seismic-Resistant Design of Buildings (4th edition, Standard 2800) [46]. High deformation without substantial strength or stiffness degradation is expected for this type of frame.

The buildings' configurations were designed according to the recommendations of Shakib and Pirizadeh [31] to consider irregularities. The story height and bay widths of both buildings, regular and irregular, are considered 3.00 m and 5.00 m, respectively. The dead and the live

loads were 7.00 and 2.00 kN/m^2, respectively, and structural occupancy was assumed for residual applications (IBNC, 2014c) [47]. Referring to Standard 2800, seismic weight includes 100% of the dead load and 20% of the live load (IBNC, 2014a) [48]. All beams and columns for both the irregular and regular structures were designed according to the Iranian Steel Design Code, which is based on the force-based approach using the load and resistance factor design method (LRFD) (IBNC, 2014c) [47].

The frame elements were made of conventional steel profiles with yield strength, ultimate strength, and modulus of elasticity of $F_y = 240$ MPa, $F_u = 370$ MPa, and $E = 200$ GPa, respectively. The beam section ranges were from 2IPE270 to 2IPE300 and box sections from 0.34 × 0.34 × 0.03 m to 0.36 × 0.36 × 0.03 m assigned to the column elements. Fig. 1 shows the 3D view and plan view of the reference structure. Moreover, in the design step, the P-delta effects were considered, however, vertical components were not normally considered in practical design approaches because all structures do not include cantilever elements and heavily concentrated forces. The geometric representations of interior frames with setbacks were similar to the reference frame.

The level of irregularity is defined by parameters including R_A (the area setback ratio) and R_H (height setback ratio). The R_A is calculated as the number of removed bays in each story divided by all bays on that level and the R_H is calculated as the number of removed stories divided by all stories [31]. These groupings were used to develop a comprehensive comparison between the seismic response of the regular and irregular frames with SATMDs. Fig. 2 shows the elevation views of steel frames with different setback irregularities. Eqs. (1) and (2) present both parameters for the 9th frame configuration, (See Fig. 2) (R_A = 0.75_R_H0.70):

$$R_A = \frac{\text{Removed bays}}{\text{All bays}} = \frac{3}{4} = 0.75 \tag{1}$$

$$R_H = \frac{\text{Removed Stories}}{\text{All Stories}} = \frac{7}{10} = 0.70 \tag{2}$$

To develop the numerical models and perform the nonlinear time history analysis of frames, the OpenSees software was used [49]. The laboratory results of an experimental test on a one-bay and one-story steel frame were used to calibrate the numerical model with the experimental test. To simulate the numerical model of the experimental test on the steel, the frame and cross-section geometry characteristics of the experimental test were used. The Steel01 material from the material library of Opensees was assigned to the beam and column section of the steel frame.

Steel01 material was introduced as a uniaxial bilinear material with kinematic hardening. The yield strength and hardening ratio for the steel material of the studied frame are considered, 315 MPa and, 0.15, respectively. The beam and column of the frame for the experimental test were IPE 140. To simulate the numerical model for the frames Fiber Section and Nonlinear Beam-Column were used for the cross-sections and elements of the frames. All column-based were considered fixed and the rigid diaphragm was assigned to the roof of each story. In addition, the beam length and column height of the experimental test were 2.40, and 1.87 m, respectively. Fig. 3 (left) shows the experimental and numerical results and the comparison shows a good fitting between the numerical and experimental tests [50].

Moreover, the modal and nonlinear seismic response of the numerical model was compared with the result of a shaking table test. Kim et al. [51] experimentally studied the seismic behavior of a two-story one-bay full-scale steel moment-resistant frame under the Northridge earthquake (90,055 Simi Valley-Katherine Rd). All beams and columns are made of steel material with grade SS400. The hot rolled wide flange section (H 125 × 125 × 9 × 6.5 mm) was used for all structural elements. The Rayleigh damping was considered 5%. Table 1 shows the first and second periods of the structure which depict the accuracy of the modal analysis. In addition, assuming this damping was used in other numerical studies with different approaches for the same experimental test [52,53].

Furthermore, the maximum relative displacements for the numerical model and laboratory study under the mentioned seismic event have a good agreement with an error equal to 1.89% and 7.78% for the first and second floors, respectively. Fig. 3 (right) shows the comparison of the time history of the relative displacement of the second floor for both numerical and experimental models. This figure shows that the numerical model has not only a nearly close time history behavior during the dynamic analysis but also the residual displacement due to material and geometry nonlinearity is close to the experimental test.

In the first stage, for all irregular and regular case study structures, both modal and push-over (non-linear static) analyses were performed to determine the dynamic characteristics and structural capacity, respectively. The capacity curves of structures were derived by pushover analysis by applying the lateral first mode force pattern. Fig. 4 (left) shows the capacity curves (base shear normalized by the frame seismic weight, V_b/W, versus roof drift ratio) drawn from the results of nonlinear static analysis of the regular and irregular structural models.

The parameters depending on the yielding point of structures, yield drift ratio (Θ_y), and coefficient of yield strength (C_y), were calculated by developing a bilinear capacity curve of structures. The stiffness of the first and second lines of the bilinear carve is driven by the initial and ultimate slope (stiffness) of the capacity curve (Fig. 4 right). Table 2 lists the fundamental period of vibration (T_1), yield drift ratio (Θ_y), and coefficient of yield strength (C_y) for the reference frame and irregular frames with setbacks.

Fig. 4 (left) and Table 2 show that, as the setback parameter values increased, especially when R_A and R_H were >50%, the capacity of the irregular structure was significantly less than for the reference frame. For example, parameters Θ_y and C_y for the reference frame were 1.2 and

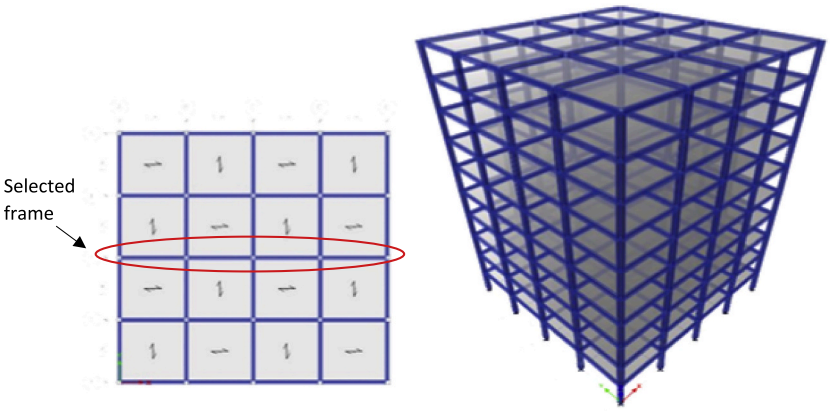

Fig. 1. 3D view and plan of reference frame.

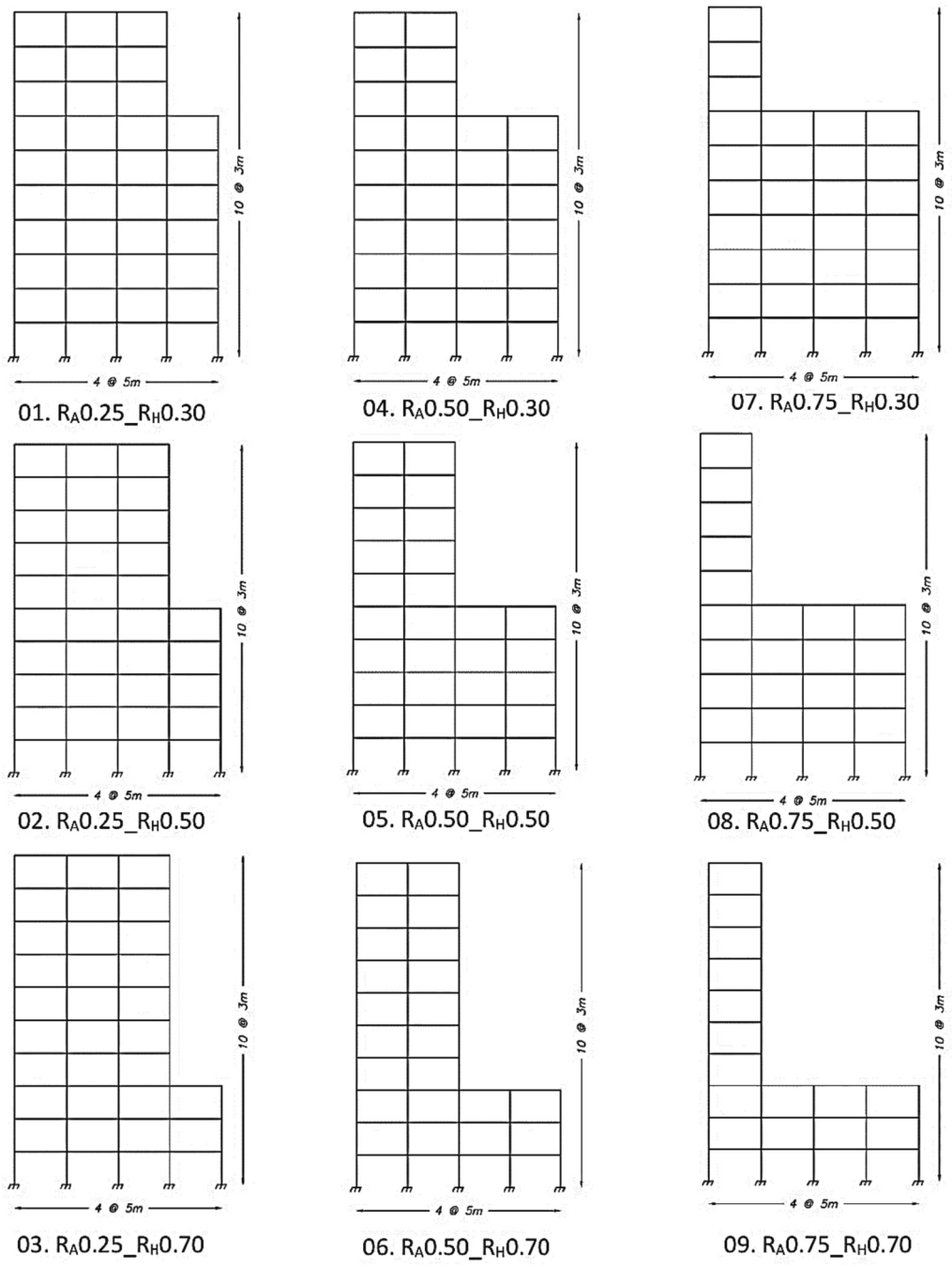

Fig. 2. Steel frames with different setbacks.

0.15 and for the irregular frame (No. 09) they were 0.70 and 0.06, respectively. Also, with increasing the setback of structures, the fundamental period of vibration of structures was reduced, however, normally standards use the height of the structure to calculate the period of structures [46,54].

After that, nonlinear time history analyses were carried out to determine the seismic response of both types of frames under uncontrolled and controlled conditions.

To perform nonlinear time history analyses, based on the Iranian Seismic Design Code (Standard 2800) [46], seven strong ground motions were selected from the PEER-NGA database [55]. These earthquakes have similar seismic characterization as the Standard 2800 suggestions. Table 3 presents information on the seismic characterization of selected ground motion records.

Regarding Standard 2800, the soil class chosen was type III ($175 < V_{s30} < 375$ m/s). In the first stage, seismic events with limitations such as an average soil shear-wave velocity of $175 < V_{s30} < 375$ m/s and a relatively strong ground motion of large magnitude ($6 < M < 7.6$) were selected. Considering the far-field features of the earthquakes, the selected events did not have pulse-like effects. In addition, the distance to the fault rupture was >20 km ($R > 20$ km).

Fig. 5 (left) shows the standard spectrum of the Iranian Seismic Design Code (Standard 2800) [46], lower bound spectrum, design spectrum, and the average elastic spectrum of selected earthquakes (damping = 5%). Fig. 5 (left) shows that the selected earthquakes have a close trend with the standard spectrum and between the mentioned periods their spectral acceleration (S_a) is bigger than the lower bound limitation. Fig. 5 (right) shows the spectral displacement (S_d) and the

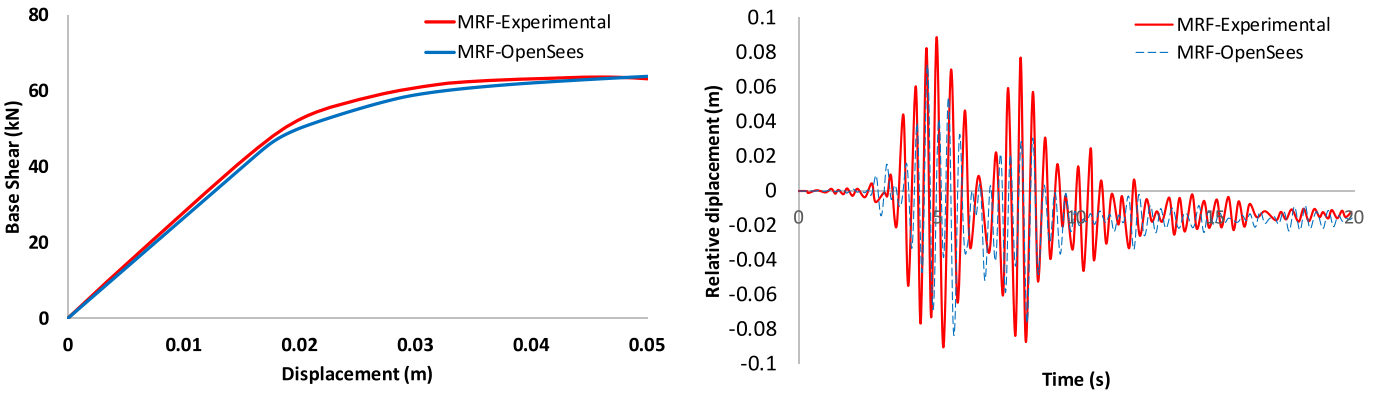

Fig. 3. Results of the push-over (left) and time history (right) analysis for numerical (OpenSees) and experimental models.

Table 1
Verification of modal and seismic behavior of steel frame.

Analysis	Modal		Seismic	
Parameter	Natural period (Sec)		Maximum relative displacement (m)	
	1st mode	2nd mode	1st story	2nd story
Experimental	0.393	0.112	0.053	0.090
Numerical	0.396	0.113	0.052	0.083
Error (%)	0.76	0.89	−1.89	−7.78

average S_d of the selected earthquakes. In addition, it is worth mentioning that all recodes were scaled with PGA between 0.35 g to 0.40 g. These scales are not only close to the recommended PGA = 0.35 g, for the high-risk seismic zone, but also in this situation, the response spectrum of the recodes matches with the standard spectrum.

Eq. (3) is recommended to calculate the fundamental period of steel moment resistance frames (T) without considering the effect of infilled walls on the fundamental period [46]:

$$T = 0.08H^{0.75} = 1.03\ \text{Sec} \tag{3}$$

where the H is the total height of the structure which in this study is equal to 30 m. Consequently, selected earthquake waves, between the period of 0.2 T and 1.5 T which are 0.21 and 1.54 s respectively, shall be >0.90% of the standard spectrum [46]. In addition, the design spectrum is calculated by Eq. (4):

$$\text{Design spectrum} = \frac{S_a.I}{R_u} \tag{4}$$

where S_a is defined as the value of the standard spectrum, I is an important factor equal to 1.0 for residential buildings and R_u is a behavior factor equal to 7.5 for special steel moment-resistant frames [46].

It is noticeable that as the setback ratio of structures increased, the fundamental period of structures with irregularity decreased (see Table 2), however, seismic standards [46,54] just use the height of the structure to calculate the fundamental period of structures. It means that as the setback increases, the period of structures reduces and consequently, the result will observe an increase in the spectral acceleration (Fig. 5). This result shows that to design structures with setbacks, the designer should pay attention to the changes, normally increase in the spectral acceleration parameters.

In order to reduce the lateral vibration of structures, four semi-active strategies have been proposed by the reference [56]. The displacement

Table 2
Dynamic and mechanical properties of frame models.

Frame model	T_1 (s)	Θ_y (%)	C_y
00.Reference	1.92	1.2	0.15
01.R_A0.25_R_H0.30	1.78	1.1	0.13
02.R_A0.25_R_H0.50	1.77	1.0	0.12
03.R_A0.25_R_H0.70	1.81	1.0	0.12
04.R_A0.50_R_H0.30	1.64	1.0	0.12
05.R_A0.50_R_H0.50	1.58	1.0	0.11
06.R_A0.50_R_H0.70	1.68	1.0	0.11
07.R_A0.75_R_H0.30	1.47	1.0	0.11
08.R_A0.75_R_H0.50	1.33	0.7	0.07
09.R_A0.75_R_H0.70	1.35	0.7	0.06

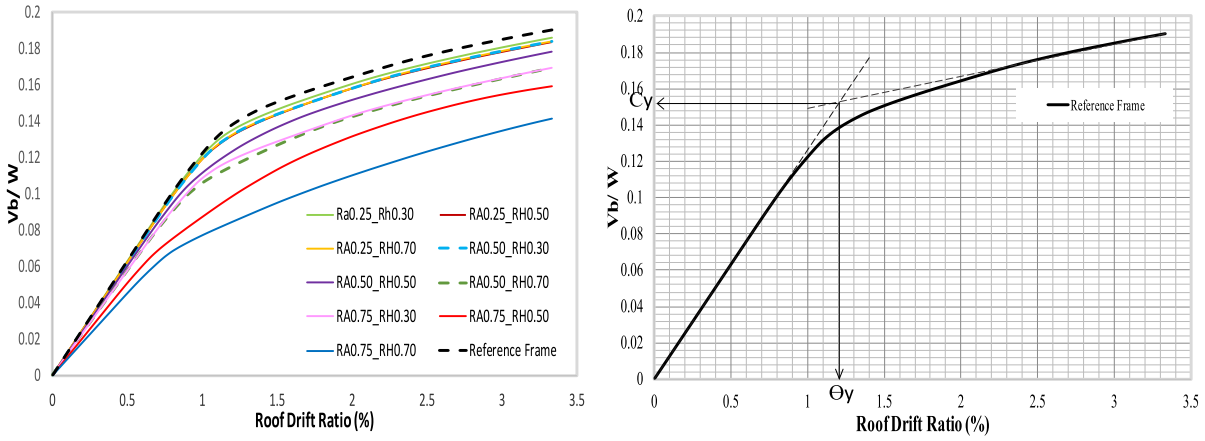

Fig. 4. Capacity curves, V_b/W VS. roof drift ratio of frames (left), an example of finding the yielding point parameters (right).

Table 3
Seismic characterization of selected ground motion records (PEER-NGA database) [55].

No.	Event name	Year	Station	Magnitude	R (km)	V_s30 (m/s)
1	Northridge-01	1994	Lawndale—Osage Ave	6.69	39.91	311.86
2	Landers	1992	Thousand Palms Post Office	7.28	36.93	333.89
3	Landers	1992	North Palm Springs Fire Sta #36	7.28	26.95	367.84
4	Kobe	1995	Yae	6.9	27.77	256.00
5	Imperial Valley-06	1979	El Centro Array #13	6.53	21.98	249.92
6	Morgan Hill	1984	Fremont-Mission San Jose	6.19	31.34	367.57
7	Loma Prieta	1989	Salinas-John & Work	6.93	32.78	279.56

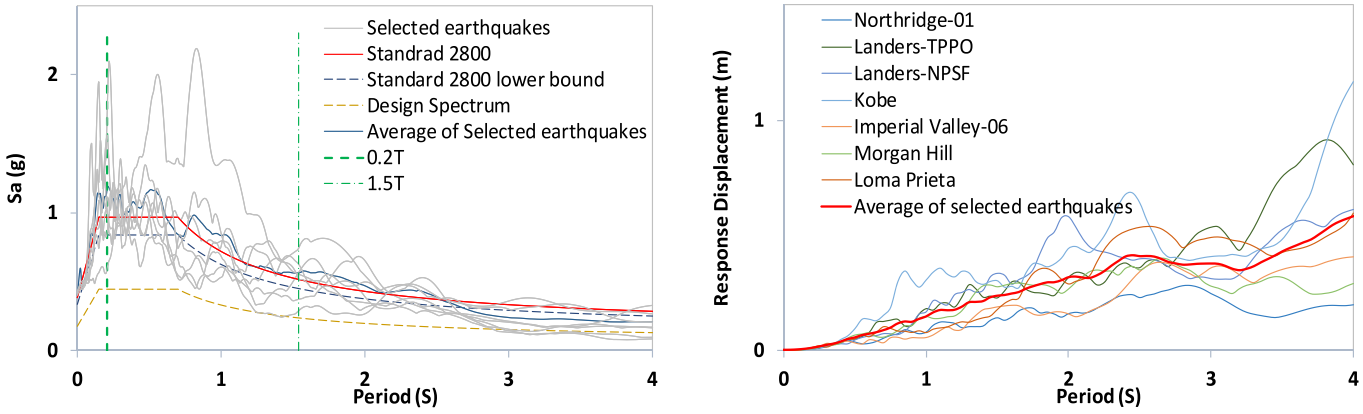

Fig. 5. Spectral acceleration (left) and spectral displacement (right).

based on on-off ground-hook control (on-off DGB) was the most suitable scheme and led to the positive control of the structural vibration [56]. The structural mass displacement and relative damper velocity were used to determine the level of on-off DBG damping as(Eq. (5)):

$$\begin{aligned} x_1 v_{12} \geq 0 \quad & \text{ccontrollable} = \text{con} \\ x_1 v_{12} < 0 \quad & \text{ccontrollable} = \text{coff} \end{aligned} \tag{5}$$

where x_1 is the structure mass displacement and v_{12} is the relative damper velocity [56]. In on-off DGBs, the damper is controlled in the on-state as well as the off-state. Fig. 6 (left) illustrates the Ground-hook damper lumped-parameter scheme with two bodies in which bodies 1 and 2 represent the structure and the controller devices, respectively. Fig. 6 (right) shows two states (on and off) damping values for seismic analysis [56].

The dynamic equation of motion for controlled structures with SATMD devices with Ground-hook equivalent configuration was derived based on a system with two degrees of freedom (Eq. (6)):

$$\begin{bmatrix} m_1 & 0 \\ 0 & m_2 \end{bmatrix} \begin{Bmatrix} a_1 \\ a_2 \end{Bmatrix} + \begin{bmatrix} c_1 + c_{controllable} & -c_{controllable} \\ -c_{controllable} & c_{controllable} \end{bmatrix} \begin{Bmatrix} v_1 \\ v_2 \end{Bmatrix} + + \begin{bmatrix} k_1 + k_2 & -k_2 \\ -k_2 & k_2 \end{bmatrix} \begin{Bmatrix} x_1 \\ x_2 \end{Bmatrix} = \begin{bmatrix} F \\ 0 \end{bmatrix} \tag{6}$$

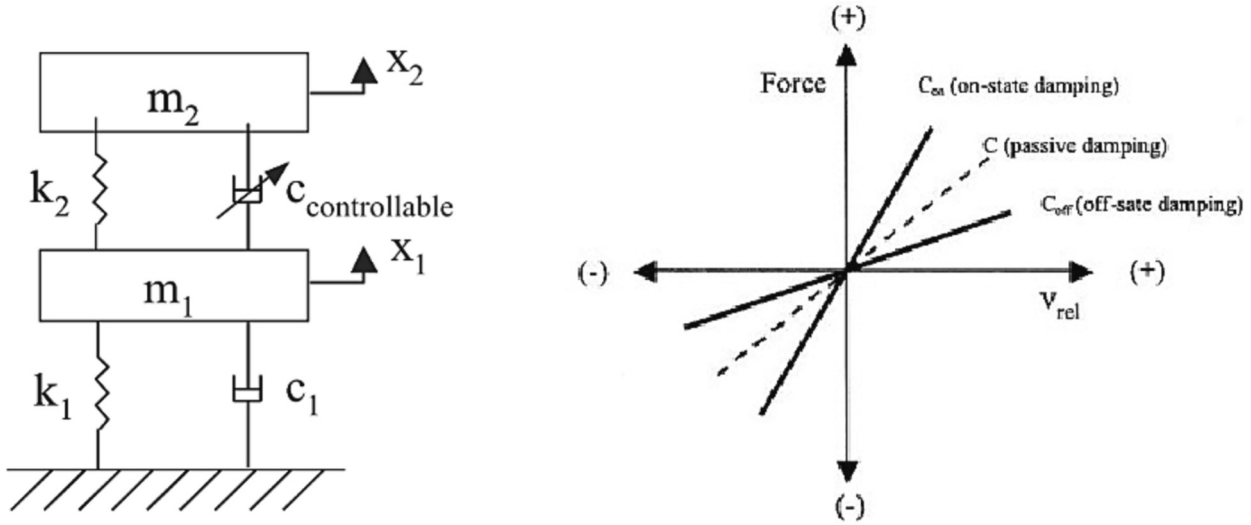

Fig. 6. Ground-hook absorber scheme (left) and force versus velocity limitations state for SATMD devices [56].

where subscripts 1 and 2 are related to the main structure and damper device, respectively. The acceleration, velocity, and displacement of each body are represented in a, v, and x in turn. The mass, damping, and stiffness of both parts are defined by m, c, and k, respectively. It is noticeable that the term controllable depends on the damper state and can be one of the minimum or maximum damping ratios. Finally, the applied action is represented by F [56].

Different position of the moving bodies, main structures, and SATMD devices, leads to generating the acting forces from the damper to the main structure. Ground-hook logic is illustrated in Fig. 7 including four possible situations. These situations related to the main structure displacements, x_1, and relative velocity, $v_{12} = v_1\text{-}v_2$, between the velocity of the main structure, v_1, and damper,v_2. The mentioned four possible situations are explained below:

I. The main body moves upwards and if the velocity of the SATMD is bigger than the velocity of the main structure, the damper has an off-state situation with minimum damping
II. The main body moves upwards and if the velocity of the SATMD is less than the velocity of the main structure, the damper has an on-state situation with maximum damping
III. The main body moves downwards and if the velocity of the SATMD is bigger than the velocity of the main structure, the damper has an on-state situation with maximum damping
IV. The main body moves upwards and if the velocity of the SATMD is less than the velocity of the main structure, the damper has an off-state situation with minimum damping

To calculate the force of the SATMD on the structure during the analysis, first, the story displacement where SATMD is attached,x_1, is calculated. Meanwhile, the relative velocity in the spring of the damper was calculated, by considering the velocity in the damper,v_2, and the velocity of the story,v_1, where the damper is attached. Finally, based on the logical equations (Eq. (5) and Fig. 7) one of each damper-state will be selected to calculate the applied force from the damper to the main structure.

The optimal frequency ratio, $f_{opt} = f_{TMD}/f_{structure}$, of the passive TMD is calculated by the empirical formulation, Eq. (7), and then Eq. (8) was used to have a preliminary evaluation of the optimal damping ratio ξ_{opt}. The empirical equation for f_{opt} and ξ_{opt} are shown in the Eqs. (7) and (8) [57–59]:

$$f_{opt} = \frac{1}{1+\overline{m}} - \left(0.241 + 1.7\overline{m} - 2.6\overline{m}^2\right)\xi_s - \left(1 - 1.9\overline{m} + \overline{m}^2\right)\xi_s{}^2 \tag{7}$$

$$\xi_{opt} = \left(\frac{3\overline{m}}{8(1+\overline{m})}\right)^{0.5} + \left(0.13 + 0.12\overline{m} + 0.4\overline{m}^2\right)\xi_s - \left(0.01 + 0.9\overline{m} + \overline{m}^2\right)\xi_s{}^2 \tag{8}$$

where $\overline{m}$ is the damper mass ratio and ξ_s is the structural damping ratio. The damper mass ratio for conventional dampers is equal to 2% [26,58,60,61], and based on verification in this study, the structural damping equal to 5% was assigned to the main structure.

The optimal frequency ratio and damping ratio for the passive damper are equal to 0.96 and 0.09, respectively [17,57]. It is worth mentioning that the optimal frequency calculated by the empirical formulation is in good agreement with the proposed optimal frequencies in the reference [52].

The maximum and minimum damping ratios of $2\zeta_{opt}$, and 0, respectively were considered by Wang et al. [25] and Ghorbanzadeh et al. used the 0.02 and 0.18 for a 7-story building [26]. In this study, to calculate the upper state parameter of damping, the on-state, value equal to 0.15 was selected refer to reference [60] then the lower state, off-state, equal to 0.03 was calculated by using the optimum damping ratio. The average value of the upper and lower states is approximately equal to ξ_{opt} and both upper and lower state values are in the range of the previous studies [56,57].

To simulate the performance of SATMD for controlling structural vibrations in OpenSees, a concentrated mass equal to the mass of SATMD is connected to the main structure by a Zero-Length element. The stiffness of the Zero-Length element is calculated based on the f_{opt} and based on the logical condition of the TMD and the main structure, Fig. 7, the damping ratio of the SATMD adopts a value of maximum or minimum in each of the on-state or off-state, respectively. In addition, the hysteretic behavior of the SATMD10, attached to the 10th story of the regular frame, is presented in Appendix A. The graph shows the applied force from the damper to the structure and the damper's

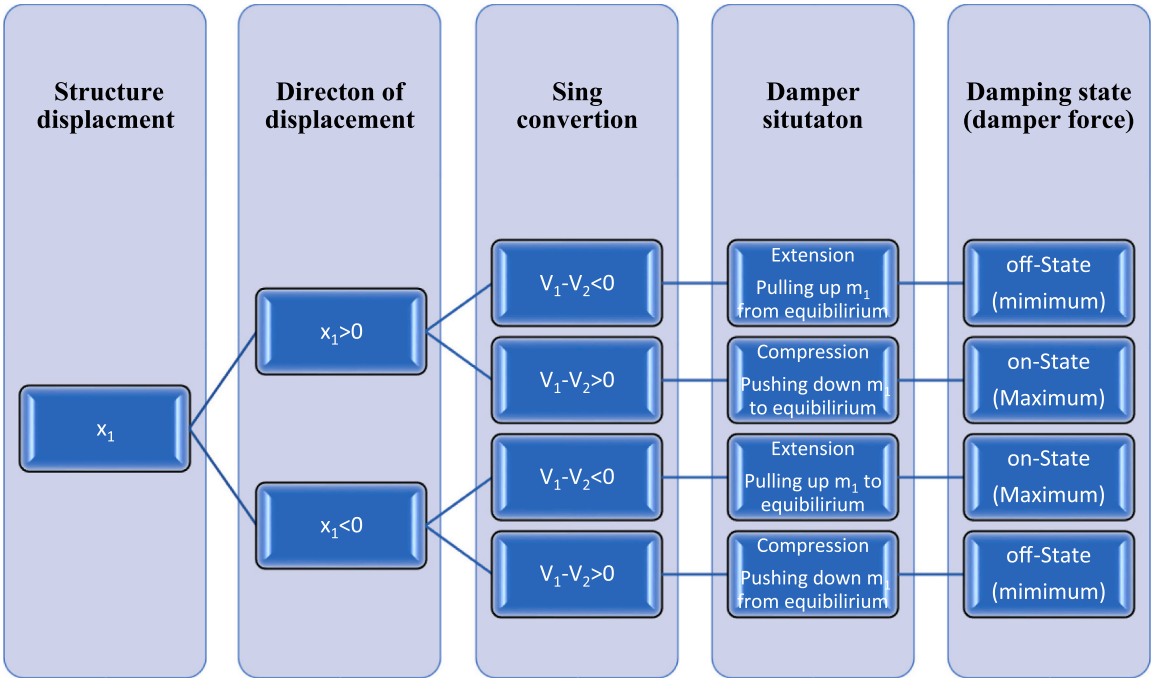

Fig. 7. Ground-hook logic.

displacement under the effect of the Northridge-01 record.

3. Vibration control of structures

This section presents the results of the efficiency of SATMD devices in reducing the seismic response of both regular and irregular structures. Five conventional engineering parameters, the inter-story drift ratio (IDR) demand, story displacement demand, story velocity demand, story acceleration demand, and base shear of the structure under the effect of selected earthquakes were studied. The SATMDs are located on different stories with one direction to evaluate the in-plane behaviors and then seven time-history analyses were performed using the selected earthquake records. The average of the maximum of each parameter is drawn as a line graph and the mean maximum base shear is calculated for each structure. The exact location of the SATMD devices is denoted as a number at the end of the SATMD statement. For example, graph SATMD1 shows the average response of the frame with a SATMD located on the first story under the effect of seven ground motions.

3.1. Inter-story drift ratios

The effect of SATMDs on decreasing the IDR demand of buildings subjected to ground motions is presented in Fig. 8. The maximum IDR demand for the uncontrolled regular (reference) structure (No. 00) and the irregular structures (No. 01, 02, 03, 04, 06, and 07) for most frames are in the middle stories (3rd to 6th). However, for irregular frames No. 05, 08, and 09, the maximum IDR demand occurred in the middle and top stories (7th to 10th), which were located above the setback stories.

Generally, the maximum IDR demand for irregular frames equipped with SATMD devices decreased obviously, which means that the SATMD devices worked efficiently. In frames, No. 00 (reference/regular), 01, 02, 03, 04, 06, and 07, the efficiency of the SATMD for reducing the IDR demand occurred in the stories in which the maximum IDR demand occurred (middle stories). For the mentioned cases, the top and bottom stories did not experience a significant decrease. In frames 05, 08, and 09, the greatest decrease in IDR occurred in stories 7, 10, and 9, respectively. It shows that the efficiency of the SATMD devices to control the seismic response of irregular frames was better than that of the reference frame (No. 00).

Furthermore, the ability of these devices to decrease the IDR is related to the location where the vibration control equipment is attached. Fig. 8 reveals that the use of SATMD devices in stories 1, 2, 3, and 4 had either a lower or negative effect on reducing IDR demand in all models in comparison with the uncontrolled models. It means that by adding SATMD devices to these stories, compared to the uncontrolled frames, a worse seismic response was recorded. For example, compared to the uncontrolled frame, when the SATMDs were located on the fourth floor and the roof, the maximum IDR demands of controlled irregular frame No.01 for story 4 decreased by 2% and 12%, respectively. However, the vibration of the middle stories decreased more than that of the top and lower stories. Furthermore, the ability of the SATMDs at different locations to control the vibration of irregular structures with setbacks (including different parameters R_A, R_H) was higher than for the reference frame (Fig. 8).

In addition, it can be seen that all irregular frames with SATMDs having dampers on the top story experienced the lowest IDR values and efficient impact during earthquake events. For example, the irregular frames (No. 01, 04, and 07) with SATMD4 (the damper located at the 4th story) and SATMD10 (the damper located at the roof) recorded the maximum IDR in the middle story (4th story) approximately a 5% and 20% decrease in the maximum IDR compared to the uncontrolled frame. However, the location of the SATMDs did not strongly affect the structural response of the regular frames as well as irregular frames. It is obvious that the dampers located on the lower stories showed limited effects on the seismic control of the irregular frames that were similar to those for the regular frame.

The maximum IDR for frames No. 00 to No.07 showed a clear trend and occurred in the middle stories (5th and 6th), nevertheless, by increasing the level of the setback, the maximum IDR trend for frames No. 08 and 09 differed. In frame No. 08, the maximum IDR values occurred in the top stories, with an increase beginning at story 5. In frame 09, the maximum IDR trend started from story 5 toward story 10 and the IDR values in the top stories were similar. It seems that the maximum IDR trend for structures with significant setback parameters ($R_A \geq 0.50$, $R_H \geq 0.50$) migrated from the middle stories toward the top stories (6th to 9th).

When R_A *was* limited ($R_A \leq 0.5$), the decrease in IDR demand had a clear pattern for irregular frames (No. 01 to 06). This pattern repeated for most cases where the SATMDs were located on different levels, however, in some cases, the maximum IDR demand of a controlled structure increased and showed no clear trend for controlling the structure (No. 07 to 09). For example, the maximum IDR demand for the regular frame and irregular frames (No.03, 06, 09) with SATMDs on stories 1 and 2 increased compared to the uncontrolled irregular frames (Fig. 8). It seems that the use of SATMDs in irregular structures requires different SATMD parameters as well as analysis under the effects of a variety of earthquake events. Fig. 8 shows that the IDR demand in irregular structures with significant setbacks ($R_A > 0.50$, $R_H > 0.50$) showed no clear trend and their seismic performance with SATMDs could not control the seismic response of the irregular structure. It means using SATMDs to control the vibration of irregular structures with significant setbacks requires more attention.

Furthermore, damage indexes measure the amount of damage to a structure. Different damage indexes have been proposed for different types of structures. In this study, the damage to frames equipped with SATMDs was measured using the HAZUS damage index according to the IDR demands [62]. Table 4 shows the relation between IDR and the HAZUS damage state for steel MRF structures that are low-rise (1–3 stories), mid-rise (4–8 stories), and high-rise structures (8+ stories). The HAZUS damage index indicated that the SATMD reduced the damage state from extensive to moderate damage (Frame No. 05, 07, and 09). Fig. 8 shows that the damage state of the controlled regular frame did not change relatively compared to the irregular frames.

Fig. 8 shows that the efficiency of SATMD for irregular buildings is more than the regular case. These results confirm that using SATMD for buildings with setbacks leads to control of the vibration of these types of structures. On the other hand, using the SATMD for irregular buildings with setbacks requires some attention because in some places it causes unsafe results. Having this type of result can be due to the effects of higher modes of vibration. The higher mode participation and seismic demand for buildings with a setback are more than regular buildings, however, in some standards, the seismic demand is underestimated [12]. When the SATMD devices are located at the lower stories the resonance phenomenon can be happened in the middle stories.

To sum up, the results depict that SATMD devices are able to control the seismic response of structures with setbacks, nevertheless, their location is highly important to have a positive performance efficiency.

3.2. Story displacement demands

The effect of the use of SATMD devices on different stories to control the maximum lateral displacement of both structure types was examined. Fig. 9 clearly shows that SATMDs could be used to control story displacement of regular frames as well as irregular frames with different setbacks. For example, a comparison of uncontrolled and controlled frames for the regular frame and irregular frame No. 06 shows that the maximum displacement of the roof decreased by about 5% and 25%, respectively. When the SATMDs were attached to the roofs of all structures, they had a better performance to reduce the lateral response of controlled structures. Fig. 9 shows that the efficiency of SATMDs on frames with moderate setback area ratios ($R_A \leq 0.25$) was not as great as for the other irregular frames.

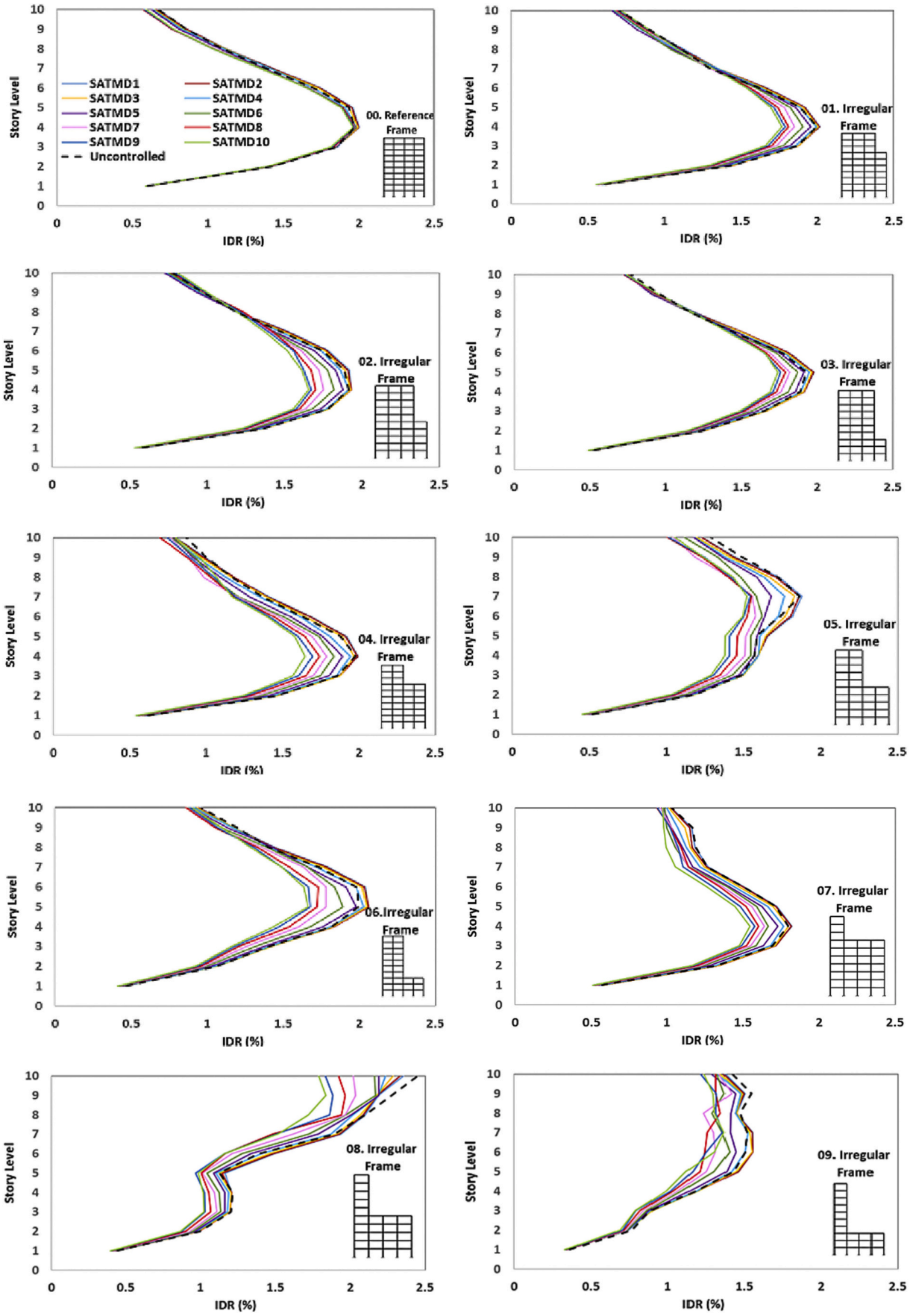

Fig. 8. Height-wise IDR demand distribution for all frames.

Table 4
IDR of MRF based on HAZUS (HAZUS, 2020) [62].

Damage state	Low-rise	Mid-rise	High-rise
Slight	0.006	0.004	0.003
Moderate	0.012	0.008	0.006
Extensive	0.030	0.020	0.015
Complete	0.080	0.053	0.040

Fig. 9 shows that the effect of SATMD location on the reduction of the story displacement demand is similar to the IDR demand. The highest story was the best place to attach the SATMD to the frames, while the efficiency of SATMDs on the first and second stories was negative. It causes a slight increase in the displacement of the stories under seismic loads. In addition, Fig. 9 shows that the SATMDs reduced the story displacement of irregular frames more than of the regular frame, 10%, and 2%, each.

It is seen that as R_A increased ($R_A \geq 0.50$), the peak displacement story (PDS) in the 4th story decreased significantly. The PDS for irregular frames No. 04, 05, 06, and 07 in the controlled structure decreased by >20%.

In most cases of controlled structures with SATMDs, except for the reference frame and irregular frames at $R_A \geq 0.75$ and $R_A \leq 0.25$ (No. 01, 02, 03, 08, and 09), after maximum story displacement was recorded, the response of the structure decreased sharply. This could depend on SATMD parameters becoming more active after reaching the peak point of the reaction.

3.3. Story velocity demands

In this section, the efficiency of the SATMD devices to control the maximum story velocity demands of structures is presented. Fig. 10 depicts the average of the maximum story velocity under the effect of selected earthquakes by considering the uncontrol and control structures. In addition, the graphs related to the location of the SATMDs are presented.

The regular building, in both uncontrol and control conditions, has less maximum story velocity, however, by increasing the irregularity in the building the velocity demand is increased. For example, the maximum velocity in the uncontrolled reference frame is equal to 1.6 m/s, however, this parameter for buildings No. 07 and 08 is close to 2.0 m/s.

Generally, the results show that using SATMD devices has a positive effect on both regular and irregular frames in terms of the story velocity demands. The average of the maximum velocity demand for all structures is reduced, by using dampers, from 3.59% to 12.38% and 4.69% to 10.10% for irregular and regular frames, respectively. Also, the efficiency of the SATMDs for buildings with high levels of setback is more than the reference frame.

Furthermore, the location of the SATMDs has a remarkable impact on the efficiency of the dampers to reduce the maximum story velocity demand. When the devices are attached to the top floor, the reduction of the maximum story velocity is up to 15.46% (for building No. 08), however, this parameter is 3.07% for the situation where dampers are attached to the first floor.

3.4. Story acceleration demands

The acceleration is a key parameter in the seismic design process for not only the structural members but also for non-structural elements such as pipelines, cable trays, and the building facade [63]. In this section, the average of the maximum story acceleration demands for both regular and irregular frames is presented.

Fig. 11 shows the acceleration demands for irregular buildings are more than the regular case. For all case studies, the maximum acceleration appears at the roof level, however, the acceleration in stories has not increased by increasing the story level. For the regular frame, the acceleration at the middle stories, 3rd to 8th, has not a big change. This figure depicts that not only the acceleration growth by increasing the irregularities level but also the acceleration pattern shows a significant increase at irregular frames. For instance, the maximum acceleration for the regular frame and irregular frames No. 07 and 08 is 9.36 m/s^2, 16.00 m/s^2, and 15.69 m/s^2, respectively.

The SATMD devices can reduce the maximum acceleration demands for all buildings. The reduction for the reference frame is from 8.40% to 9.81% and the average reduction for the irregular frames is from 7.92% to 9.72%. In addition, Fig. 11 shows that the acceleration of controlled structures has the same trend as their uncontrolled condition.

Although the SATMDs for both regular and irregular frame has a positive effect on reducing the acceleration demands, the damper's location has not a significant change in their efficiency. For example, the average acceleration reduction of irregular frames for SATMD01 and SATMD10 has 1.80% differences.

3.5. Base shear factor

The base shear factor is the maximum base shear recorded during an earthquake event over the total weight (V_b/W) for the uncontrolled and controlled frames. Fig. 12 shows that, for all models, the base shear factor for the controlled models was less than for the uncontrolled models. It can be seen that an increase in irregularity factors R_A and R_H increased the base shear factor.

The location of the SATMD will influence the base shear factor. Regardless of the irregularity factors, the best location for the SATMD was the highest level leading to efficient control of the base shear factor of the structure. Moreover, it could be seen that, as R_A and R_H increased, the difference between the base shear factors for controlled structures and uncontrolled structures decreased.

When a SATMD was added to the structure, part of the input energy from the earthquake was absorbed by the SATMD and released as input energy with damping and kinetic energy. This energy absorption decreased the IDR, story displacement, and base shear in the controlled structures.

3.6. Comparison between SATMD and TMD devices

In order to show the efficiency of SATMD (Semi-Active equipment) compared to TMD (Passive equipment), the displacement time history for the 4th story of studied frames is presented. Fig. 13 shows the time history for the 4th story of frames with SATMDs and TMDs located on the roof (SATMD10 and TMD10) under the effect of the Northridge01earthquake record. The story was selected because their graphs (Fig. 8) show that, in most cases, the maximum IDR demand was in the middle stories.

The results show that the efficiency of Semi-Active equipment in reducing the seismic behavior of controlled structures is 3% to 5% more than passive controllers (TMD). In addition, Fig. 13, declares that the differences in seismic behavior of structures with SATMD and TMD occurred at the peak displacement point. At this point, the SATMDs work more efficiently than TMDs. After that, as time increases, the structural behavior of controlled structures with semi-active and passive approaches is approximately different.

The efficiency of SATMD10 and TMD10 to control the story displacement and story acceleration demands are presented in Table 5. The results of this table are the average of the mentioned parameters under the effect of all selected earthquakes when the damper devices are located at the roof level. The efficiency of the SATMDs, compared to TMDs, to reduce the average story displacement demands and story acceleration demands, at the roof level, for all case studies is 4.28% and 2.70%, respectively. These results depict the efficiency of the semi-active devices is more than the passive devices.

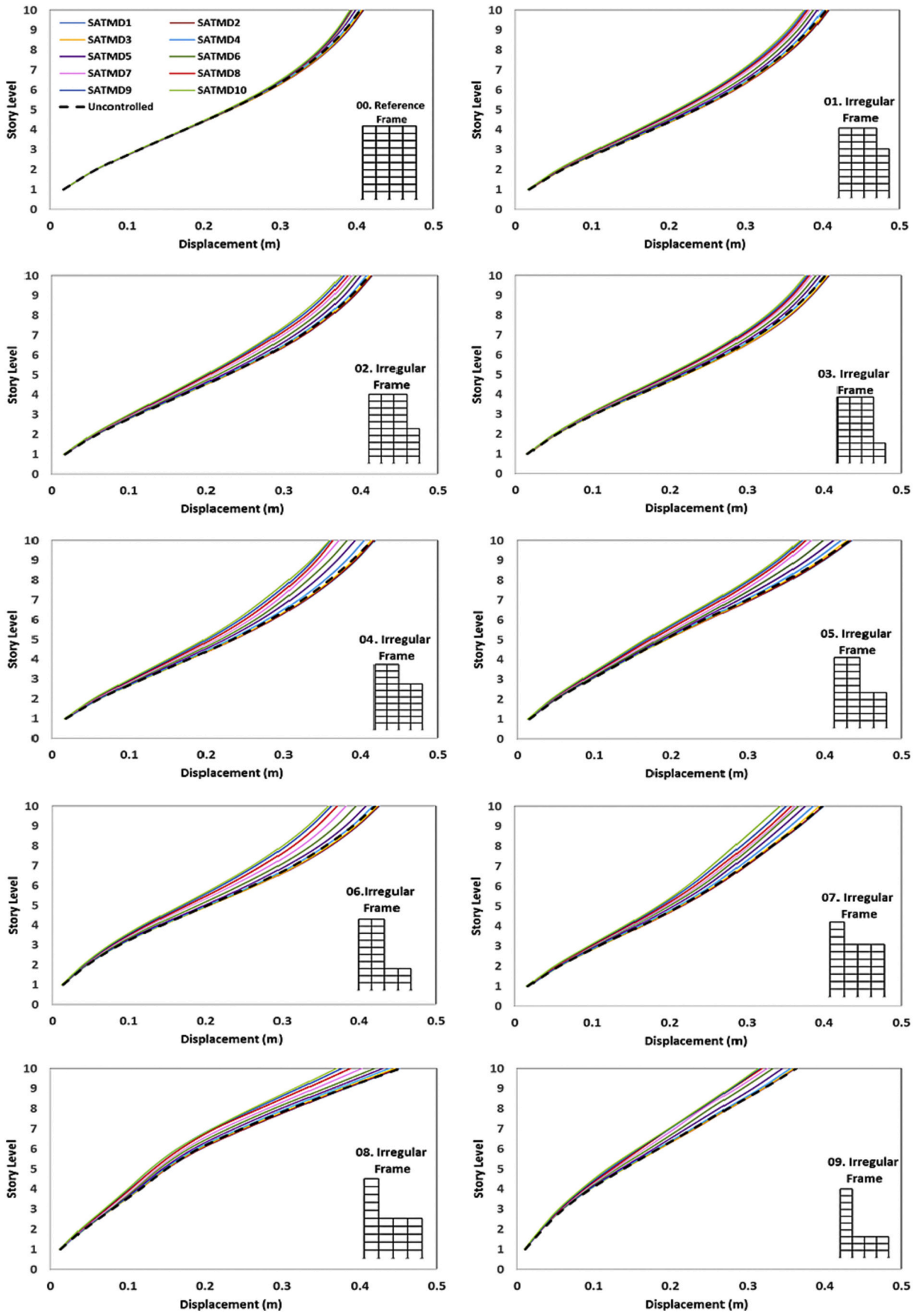

Fig. 9. Height-wise displacement demands distribution for all frames.

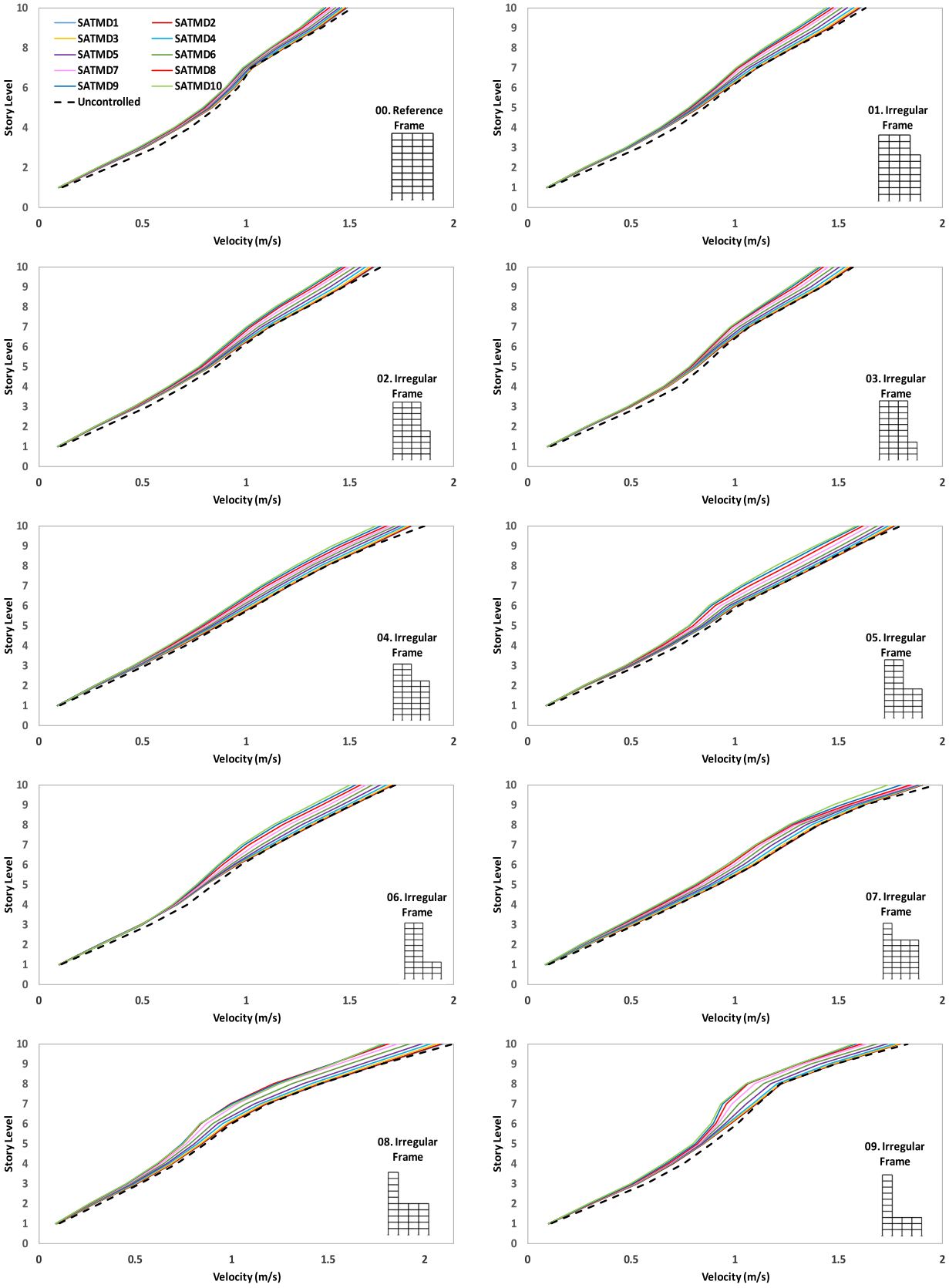

Fig. 10. Height-wise velocity demands distribution for all frames.

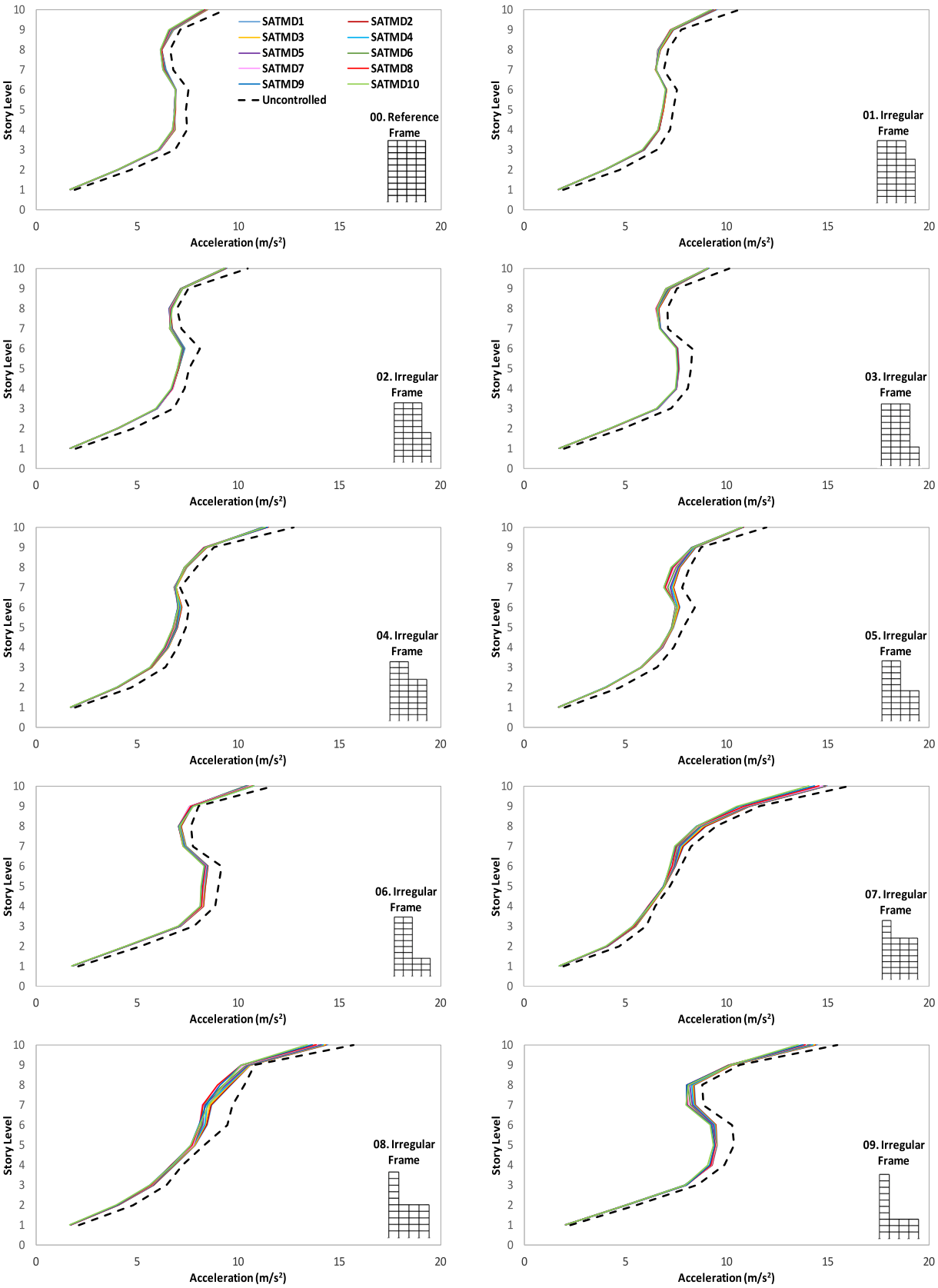

Fig. 11. Height-wise acceleration demands distribution for all frames.

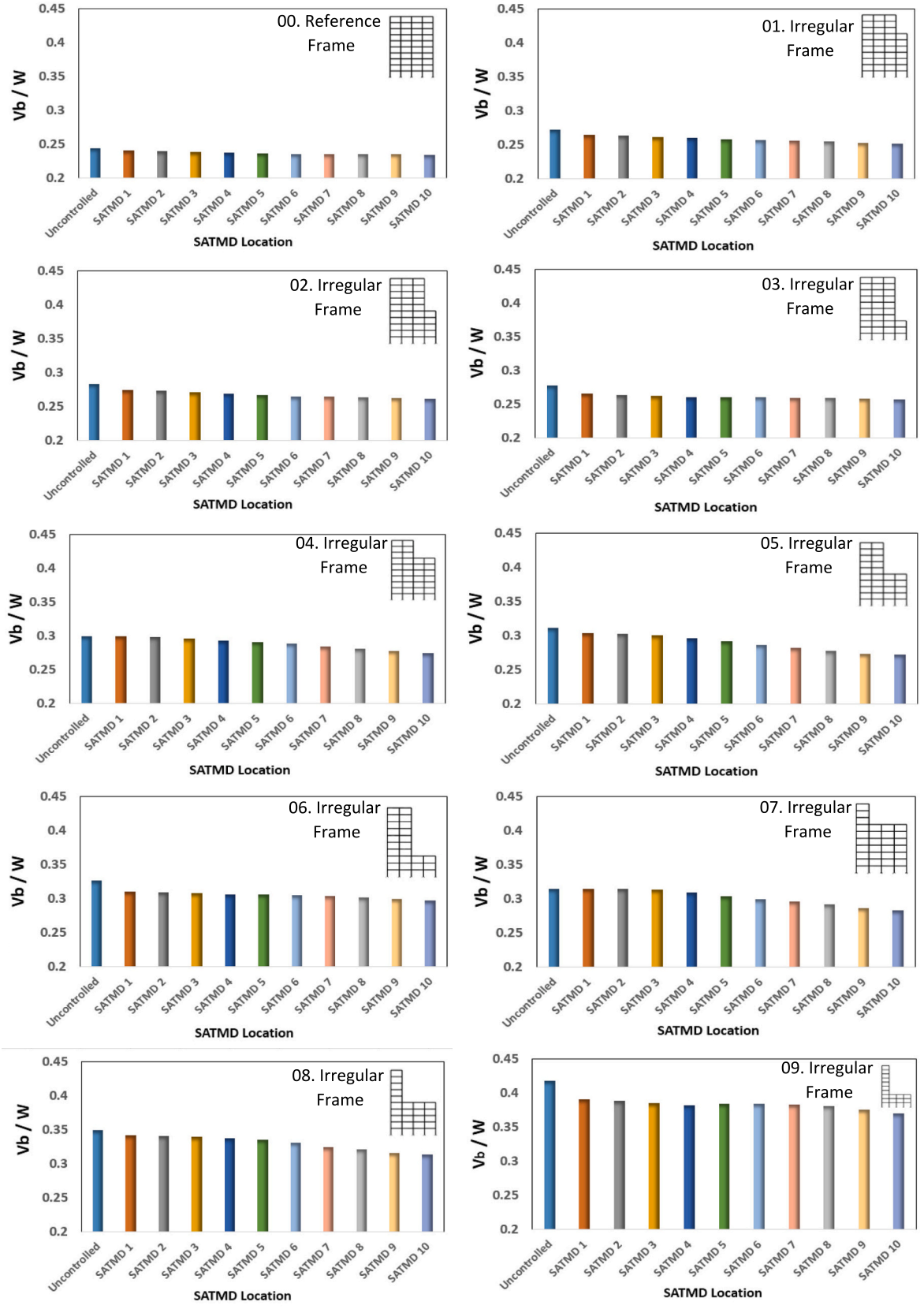

Fig. 12. Maximum base shear factor for all frames.

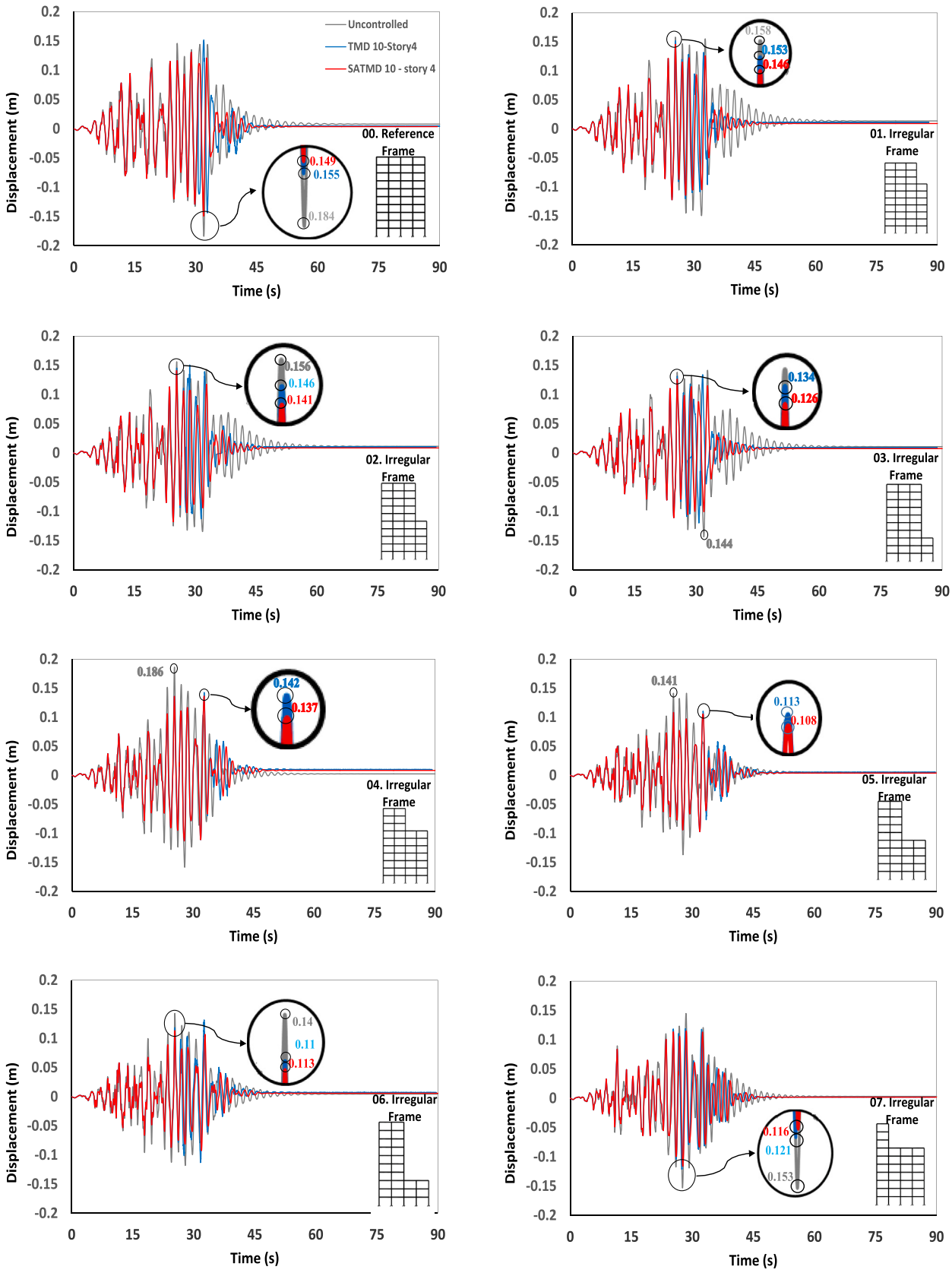

Fig. 13. Time history displacement of story 4 for TMD10 and SATMD10.

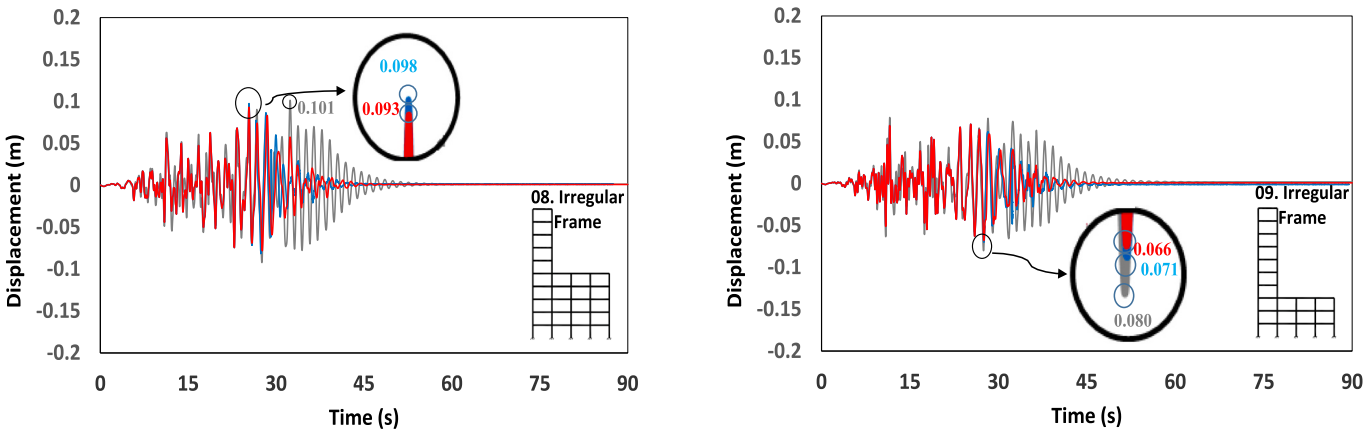

Fig. 13. (*continued*).

Table 5
Comparison between Uncontrolled structures and controlled structures with TMD and SATMD devices located at the roof.

Frame	Reference			1			2			3			4		
	U	T	ST	U	T	ST	U	T	ST	U	T	ST	U	T	ST
Disp (m)	0.405	0.396	0.391	0.404	0.387	0.376	0.411	0.389	0.375	0.401	0.386	0.376	0.415	0.378	0.359
Accel (m/s^2)	9.361	8.492	8.260	10.641	9.642	9.254	10.481	9.594	9.328	10.125	9.276	9.064	12.726	11.664	11.347
Frame	5			6			7			8			9		
	U	T	ST	U	T	ST	U	T	ST	U	T	ST	U	T	ST
Disp (m)	0.433	0.390	0.368	0.421	0.382	0.360	0.398	0.360	0.343	0.453	0.395	0.370	0.363	0.332	0.313
Accel (m/s^2)	11.964	11.034	10.772	11.727	11.014	10.751	16.033	14.528	14.052	15.694	13.897	13.419	15.479	13.989	13.518

Key:
U: Uncontrolled
T: TMD
ST: SATMD
Disp: Displacement
Accel: Acceleration

4. Conclusions

The objective of this study is to determine the efficiency of SATMD devices for controlling the seismic response of regular and irregular steel moment-resistance frames under far-field earthquake excitations. The results showed that the SATMD devices can consider an efficient approach for the control of vibrations in existing regular and irregular frames.

Generally, By increasing the setback irregularity, the fundamental period of the structure decreases. As the fundamental period of the structure is decreased, the spectral acceleration will increase. It means the seismic actions have more effect on the irregular frame with setbacks compared to regular frames.

In order to assess the effect of SATMDs on controlling the vibration of structures, the engineering demand parameters of maximum IDR, story displacement, story velocity, story acceleration, and base shear demands were considered.

The SATMD devices have better performance to control the vibration of the irregular frames with the setback, however, for all buildings the location of the SATMD is important and the roof level is the best place for the equipment. It is worth mentioning that, attaching the devices to lower stories leads to an increase the demand. This phenomenon appears due to the effect of the higher vibration modes in the irregular frames.

Using SATMD devices leads to appear more reduction in the seismic behavior of irregular frames, and consequently, in some cases, their damage state decreases from an extensive to moderate range. The maximum IDR for regular and irregular structures with limited setbacks ($R_A < 0.50$, $R_H < 0.50$) is located at the middle stories(4th to 6th), however, by increasing the level of irregularity($R_A \geq 0.50$, $R_H \geq 0.50$), the maximum IDRs move from the middle to upper stories (6th to 9th).

Both story displacement and story velocity of structures increase by increasing the story level and this trend is the same for both uncontrolled and controlled buildings. The results show that using SATMD devices have a better performance for buildings with setback.

For regular and irregular frames with limited setbacks, the story acceleration demands do have not a growing trend by increasing the story level, however, as the setback increases the acceleration pattern will change. In this situation, the story acceleration demands increase due to the higher irregularities. The results show that using SATMD equipment has an efficient effect to control the demands of story acceleration for all studied buildings, however, the location of the equipment has not a significant effect as much as the displacement and velocity of stories.

Although the base shear factor for all buildings with SATMDs, has a reducing trend for both regular and irregular buildings, the buildings with a high level of setbacks have more reduction factors. It means that in terms of story shear, controlling the buildings with high levels of setback is more efficient than regular buildings with limited irregularity.

Furthermore, the influence of SATMD and TMD to reduce displacement was recorded after the peak of the earthquake. The results show that controlling the displacement and acceleration by SATMD is better than TMD devices.

The efficiency of SATMDs to control the vibration of structures with setbacks is evaluated under far-field earthquakes, however, further studies for near-fault earthquakes are required.

CRediT authorship contribution statement

Seyed Amin Hosseini: Conceptualization, Methodology, Data curation, Writing – original draft, Visualization, Investigation, Software, Validation, Writing – review & editing. **Vahid Jahangiri:** Conceptualization, Methodology, Data curation, Writing – original draft, Visualization, Investigation, Software, Validation, Writing – review & editing. **Ali Massumi:** Conceptualization, Methodology, Visualization, Investigation, Supervision, Writing – review & editing.

Declaration of Competing Interest

The authors declare that they have no known competing financial interests or personal relationships that could have appeared to influence the work reported in this paper.

Data availability

Data will be made available on request.

Appendix A

Semi-active tuned mass dampers (SATMDs) are time-varying absorbers with controllable damping. Two levels of damping were considered for the SATMD, refer to section 2. The stiffness and mass of SATMD were fixed and the damping ratio was changed between the maximum and minimum values. The applied force from SATMD to the structure depends on the relative velocity, between SATMD and the main structure, and the main structure mass displacement. The applied force from the damper to the structure and the displacement of SATMD under the Northridge-01 event are presented in Fig. A-1. The steady behavior of the SATMD is shown in this figure. It shows that the energy dissipation of the devices had a continuous performance. In addition, the pick forces were recorded as the maximum structural response occurred.

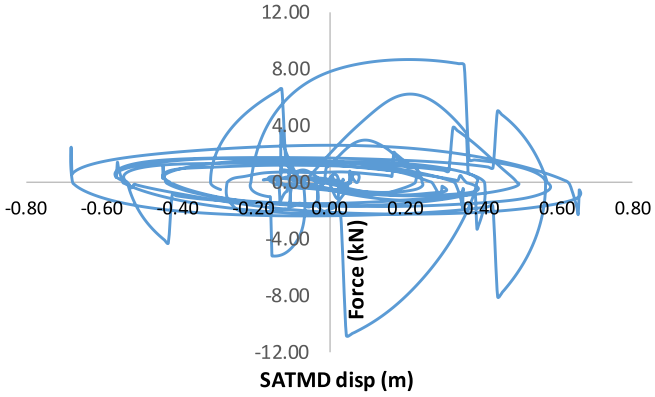

Fig. A-1. Hysteretic behavior of SATMD.

References

[1] C. Sun, S. Nagarajaiah, Study on semi-active tuned mass damper with variable damping and stiffness under seismic excitations, Struct. Control. Health Monit. 21 (6) (2014) 890–906.
[2] M.H. Chey, et al., Semi-active tuned mass damper building systems: application, Earthq. Eng. Struct. Dyn. 39 (1) (2010) 69–89.
[3] J. Kang, H.S. Kim, D.G. Lee, Mitigation of wind response of a tall building using semi-active tuned mass dampers, Struct. Design Tall Spec. Build. 20 (5) (2011) 552–565.
[4] F. Ricciardelli, A. Occhiuzzi, P. Clemente, Semi-active tuned mass damper control strategy for wind-excited structures, J. Wind Eng. Ind. Aerodyn. 88 (1) (2000) 57–74.
[5] D. Hrovat, P. Barak, M. Rabins, Semi-active versus passive or active tuned mass dampers for structural control, J. Eng. Mech. 109 (3) (1983) 691–705.
[6] N. Fisco, H. Adeli, Smart structures: part I—active and semi-active control, Sci. Iran. 18 (3) (2011) 275–284.
[7] F. Pirmoradian, A review of semi-active control in smart structures, J. Civ. Eng. Res. 1 (3) (2017) 13–21.
[8] O. El-Khoury, H. Adeli, Recent advances on vibration control of structures under dynamic loading, Arch. Comput. Methods Eng. 20 (4) (2013) 353–360.
[9] T. Pinkaew, Y. Fujino, Effectiveness of semi-active tuned mass dampers under harmonic excitation, Eng. Struct. 23 (7) (2001) 850–856.
[10] M. Setareh, Application of semi-active tuned mass dampers to base-excited systems, Earthq. Eng. Struct. Dyn. 30 (3) (2001) 449–462.
[11] C.C. Lin, G.L. Lin, J.F. Wang, Protection of seismic structures using semi-active friction TMD, Earthq. Eng. Struct. Dyn. 39 (6) (2010) 635–659.
[12] G.L. Lin, et al., Experimental verification of seismic vibration control using a semi-active friction tuned mass damper, Earthq. Eng. Struct. Dyn. 41 (4) (2012) 813–830.
[13] M.H. Chey, et al., Semi-active tuned mass damper building systems: design, Earthq. Eng. Struct. Dyn. 39 (2) (2010) 119–139.
[14] L.-L. Chung, et al., Semi-active tuned mass dampers with phase control, J. Sound Vib. 332 (15) (2013) 3610–3625.
[15] M.G. Soto, H. Adeli, Optimum tuning parameters of tuned mass dampers for vibration control of irregular highrise building structures, J. Civ. Eng. Manag. 20 (5) (2014) 609–620.
[16] H.-S. Kim, C. Chang, J.-W. Kang, Control performance evaluation of semi-active TMD subjected to various types of loads, Int. J. Steel Struct. 15 (3) (2015) 581–594.
[17] A. Bathaei, S.M. Zahrai, M. Ramezani, Semi-active seismic control of an 11-DOF building model with TMD+ MR damper using type-1 and-2 fuzzy algorithms, J. Vib. Control. 24 (13) (2018) 2938–2953.
[18] Z. Lu, et al., Shaking table test and numerical simulation on vibration control effects of TMD with different mass ratios on a super high-rise structure, Struct. Design Tall Spec. Build. 27 (9) (2018), e1470.
[19] B.S.K. Reddy, A.M. Latha, C. Srikanth, Analysis of irregular high raised RCC buildings by using tuned mass damping system, Int. J. Adv. Eng. Res. Sci. 5 (3) (2018) 237413.
[20] S. Elias, R. Rupakhety, S. Olafsson, Analysis of a benchmark building installed with tuned mass dampers under wind and earthquake loads, Shock. Vib. 2019 (2019).
[21] S. Elias, V. Matsagar, T. Datta, Distributed tuned mass dampers for multi-mode control of benchmark building under seismic excitations, J. Earthq. Eng. 23 (7) (2019) 1137–1172.
[22] M.-H. Shih, W.-P. Sung, Development of semi-active mass damper with impulsive reaction, Sādhanā 45 (1) (2020) 1–11.
[23] H.-S. Kim, Development of seismic response simulation model for building structures with semi-active control devices using recurrent neural network, Appl. Sci. 10 (11) (2020) 3915.
[24] F. Ferreira, et al., Use of semi-active tuned mass dampers to control footbridges subjected to synchronous lateral excitation, J. Sound Vib. 446 (2019) 176–194.
[25] L. Wang, et al., Seismic performance improvement of base-isolated structures using a semi-active tuned mass damper, Eng. Struct. 271 (2022) 114963.

[26] M. Ghorbanzadeh, S. Sensoy, E. Uygar, Vibration control of midrise buildings by semi-active tuned mass damper including multi-layered soil-pile-structure-interaction, in: Structures, Elsevier, 2022.
[27] H. Owji, A.H.N. Shirazi, H.H. Sarvestani, A comparison between a new semi-active tuned mass damper and an active tuned mass damper, Procedia Eng. 14 (2011) 2779–2787.
[28] B.M. Shahrooz, J.P. Moehle, Seismic response and design of setback buildings, J. Struct. Eng. 116 (5) (1990) 1423–1439.
[29] A. Osman, Seismic response of steel frames with symmetric setback, in: Urban Earthquake Risk: Proceedings of the 7th US National Conference on Earthquake Engineering, Boston, Mass, 2002.
[30] R. Tremblay, L. Poncet, Seismic performance of concentrically braced steel frames in multistory buildings with mass irregularity, J. Struct. Eng. 131 (9) (2005) 1363–1375.
[31] H. Shakib, M. Pirizadeh, Probabilistic seismic performance assessment of setback buildings under bidirectional excitation, J. Struct. Eng. 140 (2) (2014) 04013061.
[32] S. Mashhadi, et al., Fragility analysis of steel MRFs: Effects of frequency-content components of near-fault pulse-like ground motions and setbacks, in: Structures, Elsevier, 2021.
[33] T.L. Karavasilis, N. Bazeos, D. Beskos, Seismic response of plane steel MRF with setbacks: estimation of inelastic deformation demands, J. Constr. Steel Res. 64 (6) (2008) 644–654.
[34] H. Shakib, F. Homaei, Probabilistic seismic performance assessment of the soil-structure interaction effect on seismic response of mid-rise setback steel buildings, Bull. Earthq. Eng. 15 (7) (2017) 2827–2851.
[35] C.I. Nievas, T.J. Sullivan, Applicability of the direct displacement-based design method to steel moment resisting frames with setbacks, Bull. Earthq. Eng. 13 (12) (2015) 3841–3870.
[36] M. Pirizadeh, H. Shakib, On a reliability-based method to improve the seismic performance of midrise steel moment resisting frame setback buildings, Int. J. Steel Struct. 19 (1) (2019) 58–70.
[37] S. Mashhadi, F. Homaei, Soil-structure interaction and frequency components of near-fault records on the performance-based confidence levels of steel setback MRFs, Soil Dyn. Earthq. Eng. 166 (2023) 107759.
[38] X. Tu, Z. He, G. Huang, Seismic multi-objective optimization of vertically irregular steel frames with setbacks upgraded by buckling-restrained braces, in: Structures, Elsevier, 2022.
[39] R. Jarapala, A. Menon, Seismic performance of reinforced concrete buildings on hill slopes: a review, J. Inst. Eng. (India) Ser A (2023) 1–25.
[40] A.Y. Rahmani, et al., Extension of the improved upper-bound pushover analysis for seismic assessment of steel moment resisting frames with setbacks, Bull. Earthq. Eng. 20 (13) (2022) 7609–7640.
[41] A.S. Tzimas, K.A. Skalomenos, D.E. Beskos, A hybrid seismic design method for steel irregular space moment resisting frames, J. Earthq. Eng. 26 (4) (2022) 1657–1692.
[42] N. Gholizadeh, F. Fu, Seismic behaviour of multistorey steel framed tall buildings using intentionally eccentric braces, Shock. Vib. 2023 (2023).
[43] A. Saadatkhah, M.R. Chenaghlou, M. Poursha, A simplified formula for the determination of the fundamental period of mixed structures with vertical combination of different seismic resisting systems, in: Structures, Elsevier, 2023.
[44] M.Z. Kangda, S. Bakre, Performance evaluation of moment-resisting steel frame buildings under seismic and blast-induced vibrations, J. Vibr. Eng. Technol. 8 (2020) 1–26.
[45] F. Mazza, Nonlinear seismic analysis of rc framed buildings with setbacks retrofitted by damped braces, Eng. Struct. 126 (2016) 559–570.
[46] Standard No. 2800, Iranian Code of Practice for Seismic Resistant Design of Buildings, 4rd edition, Building and Housing Research Center, Tehran, Iran, 2023.
[47] IBNC, Iranian National Building Code, Part 10—Steel Design, Institute of Building National Code, 2014.
[48] IBNC, Iranian National Building Code, Part 6—Loads for Buildings, Institute of Building National Code, 2014.
[49] F. McKenna, OpenSees: a framework for earthquake engineering simulation, Comput. Sci. Eng. 13 (4) (2011) 58–66.
[50] A.A. Tasnimi, A. Mohebkhah, Investigation on the behavior of brick-infilled steel frames with openings, experimental and analytical approaches, Eng. Struct. 33 (3) (2011) 968–980.
[51] S.-E. Kim, D.-H. Lee, C. Ngo-Huu, Shaking table tests of a two-story unbraced steel frame, J. Constr. Steel Res. 63 (3) (2007) 412–421.
[52] F. Hu, G. Shi, Y. Shi, Constitutive model for full-range elasto-plastic behavior of structural steels with yield plateau: calibration and validation, Eng. Struct. 118 (2016) 210–227.
[53] P.-C. Nguyen, et al., Nonlinear inelastic response history analysis of steel frame structures using plastic-zone method, Thin-Walled Struct. 85 (2014) 220–233.
[54] P. Code, Eurocode 8: Design of Structures for Earthquake Resistance-Part 1: General Rules, Seismic Actions and Rules for Buildings, European Committee for Standardization, Brussels, 2005.
[55] PEER Ground Motion Database, Pacific Earthquake Engineering Research Center, 2023. Available from: http://ngawest2.berkeley.edu/.
[56] J.-H. Koo, et al., In search of suitable control methods for semi-active tuned vibration absorbers, J. Vib. Control. 10 (2) (2004) 163–174.
[57] T. Ioi, K. Ikeda, On the dynamic vibration damped absorber of the vibration system, Bull. JSME 21 (151) (1978) 64–71.
[58] M. Ramezani, A. Bathaei, S.M. Zahrai, Designing fuzzy systems for optimal parameters of TMDs to reduce seismic response of tall buildings, Smart Struct. Syst. 20 (1) (2017) 61–74.
[59] M. Ramezani, A. Bathaei, S.M. Zahrai, Comparing Fuzzy Type-1 and-2 in Semi-Active Control with TMD Considering Uncertainties, 2019.
[60] M. De Angelis, S. Perno, A. Reggio, Dynamic response and optimal design of structures with large mass ratio TMD, Earthq. Eng. Struct. Dyn. 41 (1) (2012) 41–60.
[61] C.-C. Lin, J.-F. Wang, Optimal design and practical considerations of tuned mass dampers for structural control, in: Design Optimization of Active and Passive Structural Control Systems, IGI global, 2013, pp. 126–149.
[62] M.-H.L.E.M. Hazus, Methodology, Earthquake Model HAZUS-MH MR5 Technical Manual, Federal Emergency Management Agency, Washington, DC, 2020.
[63] A. Filiatrault, et al., Performance-based seismic design of nonstructural building elements, J. Earthq. Eng. 25 (2) (2021) 237–269.